Engineering Science & Technology
http://ojs.wiserpub.com/index.php/EST/

Research Article

6G Broadband and High Directive Microstrip Antenna with SIW and FSSs

Uri Nissanov*, **Ghanshyam Singh**

Department of Electrical and Electronic Engineering Science, Auckland Park Kingsway Campus, University of Johannesburg, Johannesburg 2006, South Africa
Email: uri1636@gmail.com

Received: 21 May 2023; **Revised:** 11 July 2023; **Accepted:** 24 July 2023

Abstract: Sixth-Generation (6G) wireless communication networks require the fabrication of broadband and high directivity microstrip antennas to offset the high atmospheric path loss beyond 100 Gigahertz (GHz). In this paper, we designed and proposed a couple of high-gain and broadband microstrip array antennas that have been designed within a Finite Integration Technique (FIT) solver at Computer Simulation Technology Microwave Studio (CST MWS) software in a series-parallel feeding method for a resonance frequency above 107 GHz. A Substrate-Integrated Waveguide (SIW) with dual outputs has been used at these antennas and with WR-08 waveguide that covers the 90-140 GHz frequency range, while the first was without Frequency Selective Surfaces (FSSs), and the second was with the FSSs to increase the antenna directivity further. The first design was simulated with a Finite Element Method (FEM) solver at Ansys High-Frequency Structure Simulator (HFSS) to compare the simulation results of this antenna. This comparison's peak gain and Bandwidth (BW) were correspondingly 25.3 dB, 12.5 GHz, 23.1 dB, and 11 GHz from the Ansys HFSS and the CST MWS. Thus, the accuracy and the slight deviation of the compared simulation results from each other validated the offered 6G antenna designs. Therefore, after experimental verification, the proposed antennas can be employed in 6G future wireless communication networks.

Keywords: sixth-generation (6G) antennas, substrate-integrated waveguide (SIW), frequency selective surfaces (FSSs), wireless communication networks

1. Introduction

Fifth-generation (5G) wireless communication networks are initiated globally and embedded within numerous creative features. Nevertheless, 5G specs have not comprehended the needs of the emerging technologies. These embrace high reliability, short latency, high capacity, and a data rate of terabit-per-second (Tb/s) [1]. Despite this, there are attempts to improve the reliability, capacity, and data rate of 5G wireless communication networks in the sub-6 GHz band, such as Multi-Input Multi-Output (MIMO) antennae with Composite Right/Left Hand (CRLH) structure, which can improve the gain of the designed microstrip antenna, by lowering the mutual coupling and surface wave propagations between the antenna array radiators [2]-[3]. Another way to improve the antenna gain is using a multi-stage metamaterial (MtM) array with the microstrip antenna's radiator, which is used at sub-6GHz frequencies [4]-[5], where [6] the photonic control and beam-steering array with MtM array at sub-6GHz has been used, while in [7]

DOI: https://doi.org/10.37256/est.5120243071

the reconfigurable capabilities with MtM array at sub-6GHz has been used to enhance the above parameters with the described techniques [2]-[7] can be used in higher frequency ranges in future 6G wireless communication networks. Therefore, researchers pay particular attention to 6G wireless communication networks to lighten these onerous requirements that enable emerging modern technologies and applications.

6G main applications and technologies [7]-[14] should be in the Terahertz (THz) regime and will include: (1) THz cellular communication-Technologies using frequency bands below 100 Gigahertz (GHz) cannot support Tb/s links; thus, wireless 6G will support Tb/s cellular communication system for high-speed latency and ultra-low cellular communication. In addition, THz cellular communication can support intra-device radio communication, wireless fiber for backhaul, information shower, and connectivity in data centers, (2) Machine Learning (ML) and Artificial Intelligence (AI), (3) Unmanned Autonomous Vehicles (UAV) technology, (4) Holographic Beamforming (HBF) communication, (5) THz Third-Dimensions (3D) beamforming, (6) Extended Reality (XR).

The THz band is in the frequency range from around 0.1-10 THz. Researchers have not studied this field in depth due to the shortage of developments with solid-state power sources with power over 180 mW, high-directivity antennas, and power detectors at this regime. The THz band will be vital for 6G wireless communication networks for transmitting high data rates of up to 1,000 gigabit-per-second (Gb/s). Compared to the millimeter Wave (mmWave), the THz wave will tolerate high path losses due to humid atmospheric conditions, resulting in minimal communication distance propagation. This issue can be moderated by using very crowded nano-microstrip array antennas, providing high-gain antennas that allow signal propagation a few hundred meters [15]-[18]. On the other hand, some applications demand high data rates over tens of Gb/s, supplied in the THz frequencies. These implementations are (a) Sensors and Nano-devices for military defense technologies, environmental pollution control, and health monitoring, (b) Entertainment technologies, (c) High gain communication links for backhaul and fronthaul beyond 5G (B5G)/6G communication networks [16]-[20].

Ref. [21] presented the design of an on-chip SIW antenna at a nominal frequency of 0.55 THz and implemented it with commercial 65 nanometer (nm) Complementary-Metal-Oxide Semiconductor (CMOS) technology. The peak efficiency, BW, directivity, and gain obtained were 22%, 20 GHz (3.63%), 9.4 dBi, and 2.8 dB, respectively. Ref. [22] shows the design of a 0.4 THz Folded Reflectarray (FRA) antenna. This antenna included a metallic horn as a feed and a THz grid polarizer on a 127 μm Taconic TLY-5 substrate. This antenna was manufactured as an archetype THz antenna for laboratory verification. The aperture efficiency, BW, and peak directivity obtained were 33.65%, 64 GHz (16%), and 33.66 dBi, respectively. Ref. [23] shows the design of an elliptical lens antenna within the CST MWS software fed through a Leaky-Wave Antenna (LWA) for a nominal frequency of 180 GHz. This antenna was manufactured for laboratory verification with measurements. The aperture efficiency, BW, and peak directivity, obtained were more than 80%, 80 GHz (40%), and 35.8 dBi. Ref. [24] shows the design of a dipole antenna within the CST MWS software with three directors on Benzocyclobutene (BCB) and Indium Phosphide (InP) substrates for a nominal frequency of 300 GHz. This THz antenna was compared with the Ansys HFSS. The maximum directivity, BW, and gain attained were 8.44 dBi, 116 GHz (38.6%), and 8.01 dB. Ref. [25] presents the design of a V-shaped on-chip microstrip antenna with the Ansys HFSS software with a defective ground structure for a nominal frequency of 280 GHz. The engaged fabrication used a 65 nm CMOS process technology for experimental validation with an archetype THz antenna. The radiation efficiency, BW, and peak directivity obtained were 28%, more than 80 GHz (28.7%), and 5.48 dBi, respectively. Ref. [26] shows the design of a metallic lens antenna with a feeding horn and pyramidal flare at a nominal frequency of 415 GHz, and this antenna was manufactured using a low-cost metal milling process for experimental validation with the measurement with a Vector Network Analyzer (VNA). The BW and peak gain were 90 GHz (21.68%) and 29.1 dBi, respectively. Ref. [27] presents a high directivity quasi-planar reflector antenna design with a feeding horn at a nominal frequency of 412.5 GHz. This antenna was manufactured with a low-cost metal milling process for laboratory verification. The peak radiation efficiency, BW, and gain obtained were 64.9%, 175 GHz (42%), and 32 dB, respectively.

This paper presents the modeling and simulation of 6G THz microstrip antennas. The novelty of this paperwork was to design microstrip array antennas within the CST MWS software, including a SIW with dual outputs and WR-08 waveguide with or without Frequency Selective Surfaces (FSSs) with directivity, more than 22 dBi, for 6G wireless communication networks at resonance frequencies above 107 GHz.

2. Offered antenna design and analysis

2.1 *Fundamentals of SIW technology*

SIW technology [28]-[33] needs to be used at 6G antennas because at a frequency above 110 GHz, a "SubMiniature version A" (SMA) connector is not suitable because of its small size and microstrip apparatus fabrication requires very tight endurance [34]. Moreover, compared to standard 3D rectangular waveguides, slimmer substrate dielectrics preclude Transverse Magnetic (TM) modes from resonating. Therefore, only Transverse Electric (TE) modes can efficiently spread through SIW. Figure 1 describes the fundamental SIW waveguide's topology based on a dielectric laminate with its actual sizes.

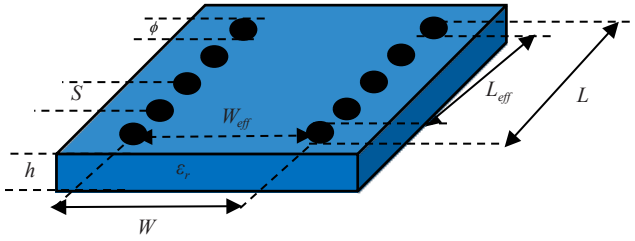

Figure 1. Fundamental topology of SIW

The design rules of the rectangular SIW are based on the first resonant frequency TE_{10} propagation mode. Furthermore, the forthcoming equations supply the TE_{10} mode for the SIW cavity [28], [32]-[33]:

$$f_{TE10} = \frac{c}{2\pi\sqrt{\mu_r \varepsilon_r}} \sqrt{\left(\frac{\pi}{W_{eff}}\right)^2} \tag{1}$$

$$\phi = \frac{\lambda_g}{5} \tag{2}$$

$$S \le 2\phi \tag{3}$$

$$L_{eff} = L - \frac{\phi^2}{0.95 \cdot S} \tag{4}$$

$$W_{eff} = W - \frac{\phi^2}{0.95 \cdot S} \tag{5}$$

Where f_{TE10} is the first resonant mode of the SIW cavity, L and W are the length and width of a single SIW cavity, ϕ is the Via's diameter, and S is the Via spacing. The guided wavelength λ_g in the SIW is given by forthcoming equations [28], [32]-[33]:

$$\lambda_g = \frac{\lambda_0}{\sqrt{\varepsilon_r \left[1 - \left(\frac{f_{TE10}}{f}\right)^2\right]}} \tag{6}$$

$$\lambda_o = \frac{c}{f_o} \tag{7}$$

Where f is the resonant frequency, c is the speed of the Electromagnetic (EM) wave in free space, ε_r is the dielectric constant of the substrate, and f_o is the resonant frequency of the antenna. This expression gives a good approximation of the TE field propagation in the SIW. We need to use a waveguide to microstrip transition to connect the radiation patch elements to the SIW. They should have broadband, low loss, and minimum Voltage Standing Wave Ratio (VSWR) properties.

2.2 *SIW at the first and second offered 6G antennas*

Figure 2 shows the designed SIW from some viewpoints.

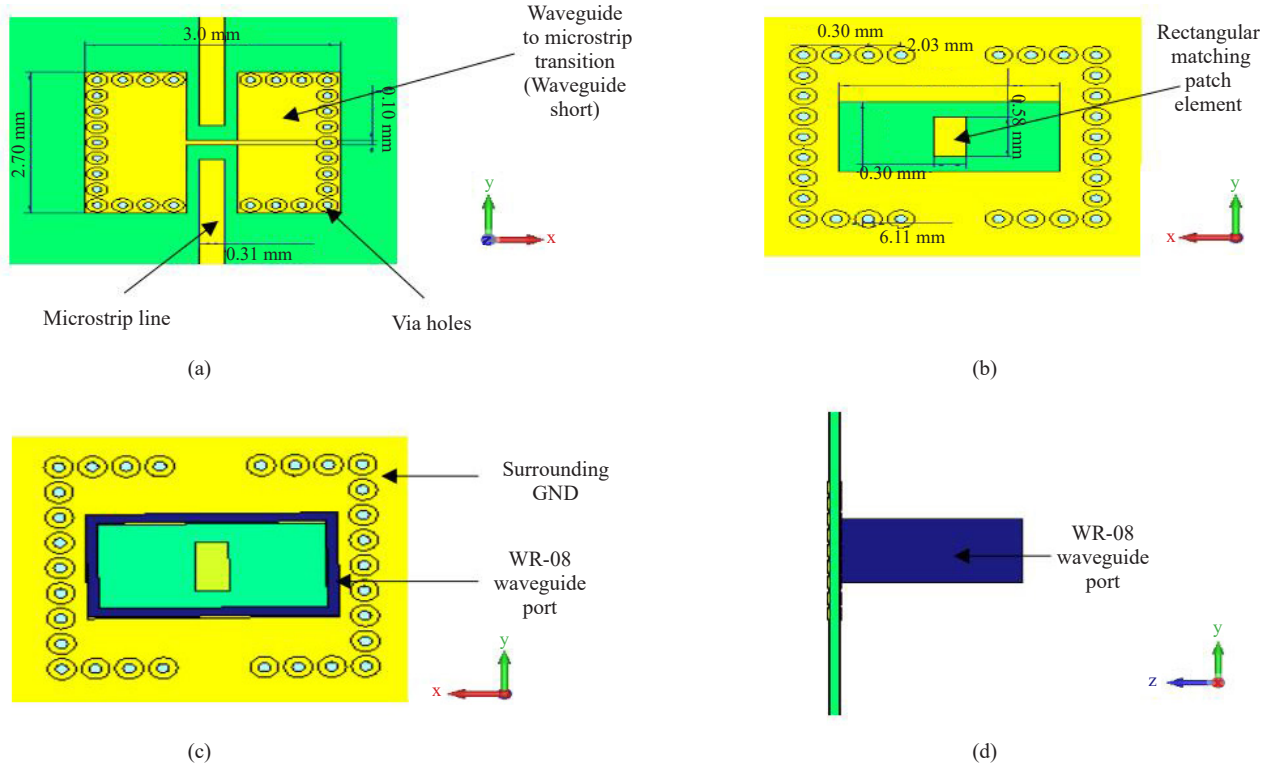

Figure 2. The designed SIW, (a) Foreground side, (b) Posterior A, (c) Posterior B, (d) Right side

Each dimension of the SIW was optimized to get the best $S_{11} \leq$ -10 dB and $S_{21} = S_{31} \leq$ -5 dB of the designed SIW. The WR-08 waveguide width and length dimensions are 2,030 × 1,020 micrometers squared (μm^2) and cover the 90-140 GHz range.

2.3 *The first offered 6G antenna*

The first offered 6G antenna is designed at one Printed Circuit Board (PCB) and contains SIW, SIW/waveguide to microstrip transition, two separate Wilkinson 1 × 16 power dividers, and two separate 20 × 16 rectangular microstrip patch radiators and presented in the following Figure 3.

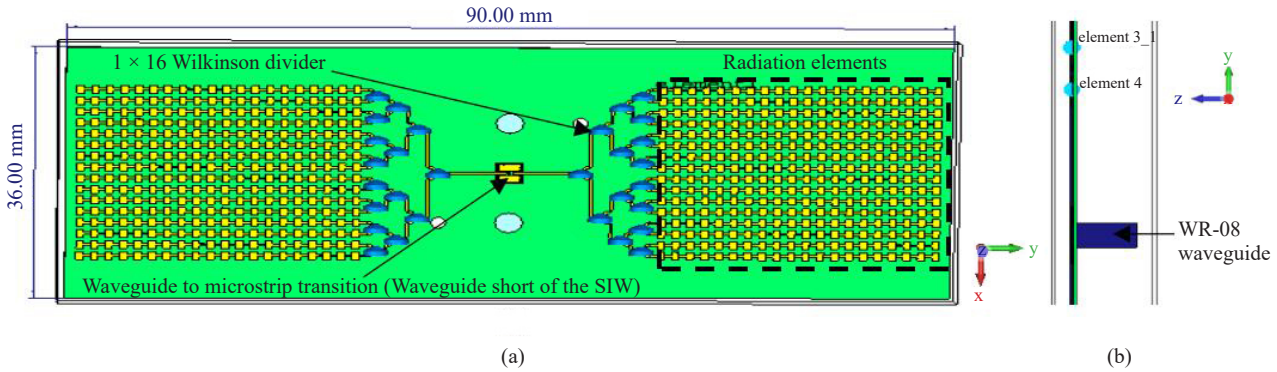

Figure 3. Structure of the first offered 6G antenna, (a) Front side, (b) Right side

Choosing the fitting microstrip laminate becomes critical at THz wavelengths due to substrate and conductor losses [34]-[37]. Microstrip arrays activated in the THz regime needing transmission lines in the feed network have lengths of approximately 40-400 μm, so high precision with tight tolerances associated with fabrication and high-cost fabrication technology is needed. Besides, numerous elements are often placed jointly in the microstrip array to achieve a high gain pattern. If we use large corporate/hybrid fed networks, that will increase the losses. Large arrays containing large antenna feed lines at corporate/hybrid fed at power dividers, which have discontinuities that introduce undesired radiation/spurious emission and interfere with its regular operation; these discontinuities are formed in the transition between the transmission line and the antenna, also at millimeter and sub-millimeter wavelengths they are a significant feed line losses because of large inductance (≈ ωL), therefore a careful selection of the feed line must be made to prevent it. The requirement to reduce this problem is to use a low-loss feed network, which is ordinary for fabricating and minimizing radiation losses in the feed line.

Numerous guidelines [34]-[37] help to reduce surface wave propagation problems and radiation losses, such as (a) A general rule by employing a substrate height (h), which is: $h \leq \lambda_{high}/8$ to remove unnecessary resonances amongst variant circuit surfaces in the PCB, where λ_{high} is the highest working wavelength of the designed antenna. (b) One approach to reducing the transmitted power from surface waves is to lower the laminate thickness to about 0.1 of the dielectric wavelength at the highest operating frequency $(h \leq \lambda_{high}/10\sqrt{\varepsilon_r})$. This parasitic radiation reduces the antenna efficiency. The right balance is achieved with ε_r of less than 3.5 and tan δ of below 0.01. (c) The conductors' width (t) is also related to a PCB substrate's thickness when a finer substrate uses a tighter (t) size. The t size should be $t \leq \lambda_{high}/8$ to reduce mode concerns.

The Rogers RO3003 laminate has been chosen, where this laminate is used up to the frequency of 100 GHz [38]-[40] and following the laminate manufacturer's declaration of the rolled copper Rogers RO3003 substrate (h = 127 μm, t = 17.5 μm, ε_r = 3.02, tan δ = 0.0019) @ 100 GHz. So with these substrate parameters, the above effects reduce to a minimum [34]-[37].

The sizes of the substrate were 90 × 36 × 0.127 millimeters in a third (mm^3) which equals $34.88\lambda_0 \times 13.95\lambda_0 \times 0.05\lambda_0$ @ 116.25 GHz, where λ_0 is the resonance wavelength of the designed antenna. Each dimension of this antenna was optimized within the CST MWS to obtain the best gain and BW for the first antenna. The FSSs were applied to increase the gain of the secondoffered 6G microstrip array antenna.

2.4 *The designed bandstop unit-cell FSS*

Figure 4 describes the structure of the designed bandstop unit-cell FSS.

The unit-cell FSS was formed within a two-printed metallic rectangular ring on Rogers RO3003 substrate within the dimensions of 1,100 × 1,100 μm^2 that equals $0.409\lambda_0 \times 0.409\lambda_0$ @ 111.7 GHz. Each parameter of the unit-cell FSS was optimized within the CST MWS to get the best reflection coefficient ($S_{11} \leq$ -10 dB) and transmission coefficient ($S_{21} \leq$ -5 dB) of this unit-cell FSS.

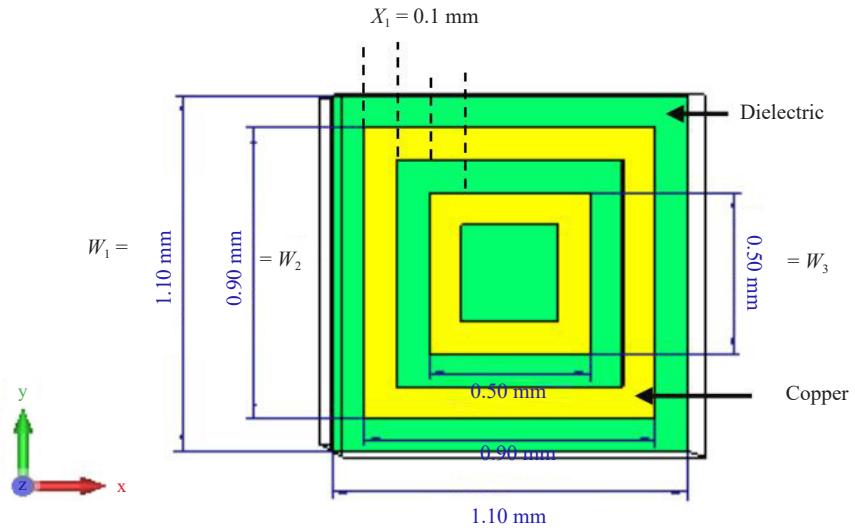

Figure 4. The bandstop unit-cell FSS

2.5 *The second offered a 6G antenna*

The second offered a 6G antenna designed at two PCBs containing FSSs superstrate with 25 unit-cell stopbands FSSs, SIW, SIW/waveguide to microstrip transition, two separate Wilkinson 1 × 16 power dividers, and two separate 20 × 16 rectangular microstrip patch radiators at the lower substrate and is presented in Figures 5(a)-(d).

Rogers RO3003 was used as the first design for the two substrates. The sizes of the laminates were 90 × 36 × 0.127 mm^3 that equals 34.87λ_0 × 13.95λ_0 × 0.05λ_0 @ 116.25 GHz. Each dimension of this antenna and the number of unit-cell stopband FSSs was optimized within the CST MWS to get this antenna's best gain and BW.

3. Simulation & comparison results and discussion

3.1 *Simulation results of the designed SIW*

Figure 6 exhibits the S_{11} and $S_{21} = S_{31}$ simulation results of the modeled SIW. From this figure, it has been displayed that the BW($S_{11} \leq$ -10 dB) of the SIW is 5.79 GHz and the $S_{21} = S_{31} <$ -4.8 dB for 106.6-112.4 GHz.

3.2 *Simulation results of the first offered 6G antenna*

Figure 7 displays the simulation result of the S_{11} of the firstoffered antenna. From this figure, it has been displayed that the BW($S_{11} \leq$ -10 dB) = 11.52 GHz (10%), while the resonance frequency is 116.23 GHz.

Figures 8(a)-(c) display the simulation results of the two-dimensions (2D) gain, 3D gain, and 3D directivity of the firstoffered 6G antenna. From Figure 8(a), it has been displayed that the gain was between 15-23.1 dB at 105-121 GHz. From Figure 8(b), the gain of this antenna was 23.1 dB @ 108 GHz, while from Figure 8(c), it has been displayed that directivity is equal to 24.95 dBi @ 108 GHz.

Figure 9 displays the simulation results of the radiation efficiency and total efficiency of the first offered 6G antenna. This figure displays that the radiation efficiency was 74.3-79.6% at 109-120 GHz, while the total efficiency was 67.7-74.4% at 109-120 GHz.

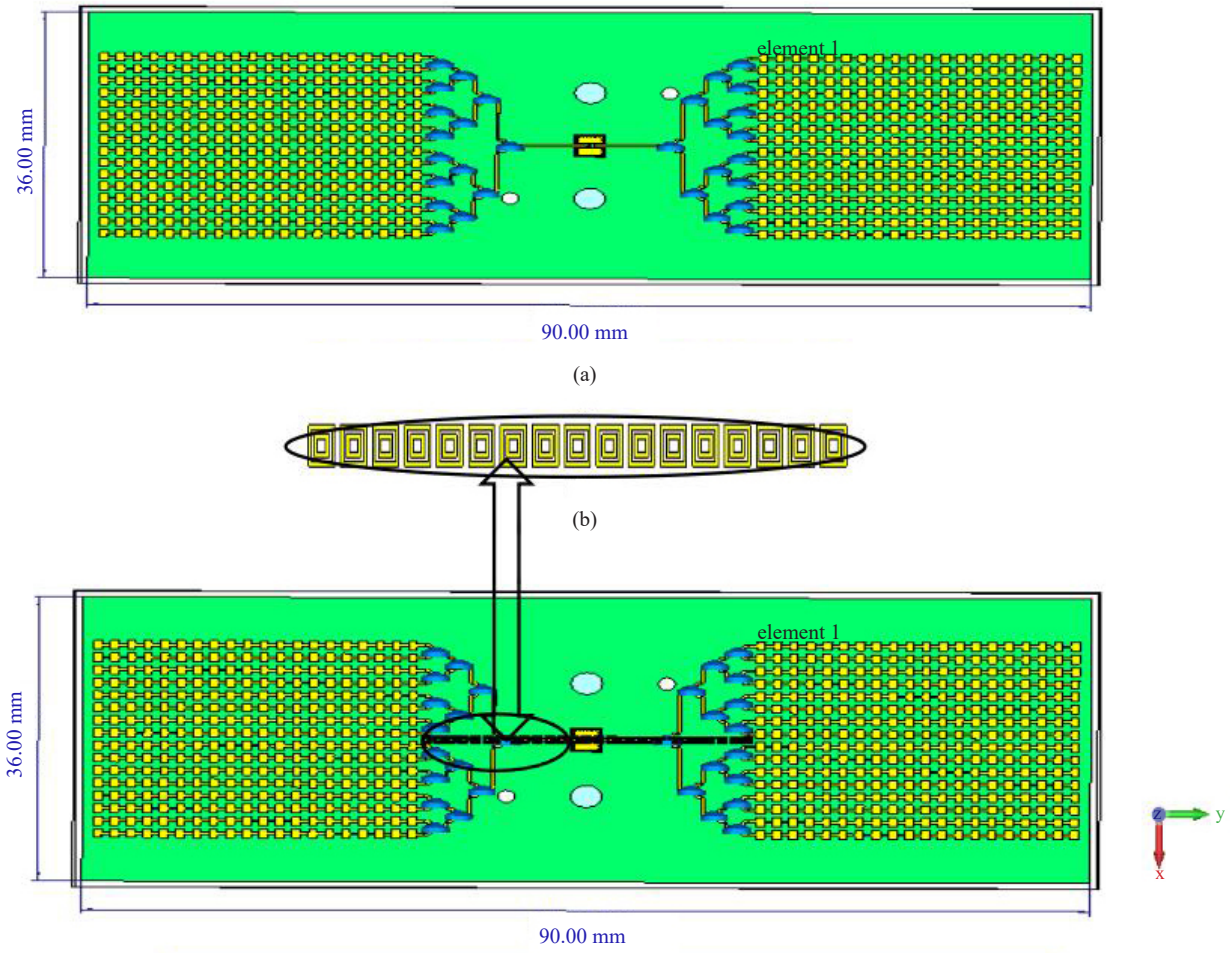

Figure 5. The second offered 6G antenna within FSSs, (a) Microstrip 6G antenna at the nether laminate, (b) Part of FSSs superstrate, (c) The secondoffered antenna, (d) A side view of the designed secondoffered antenna

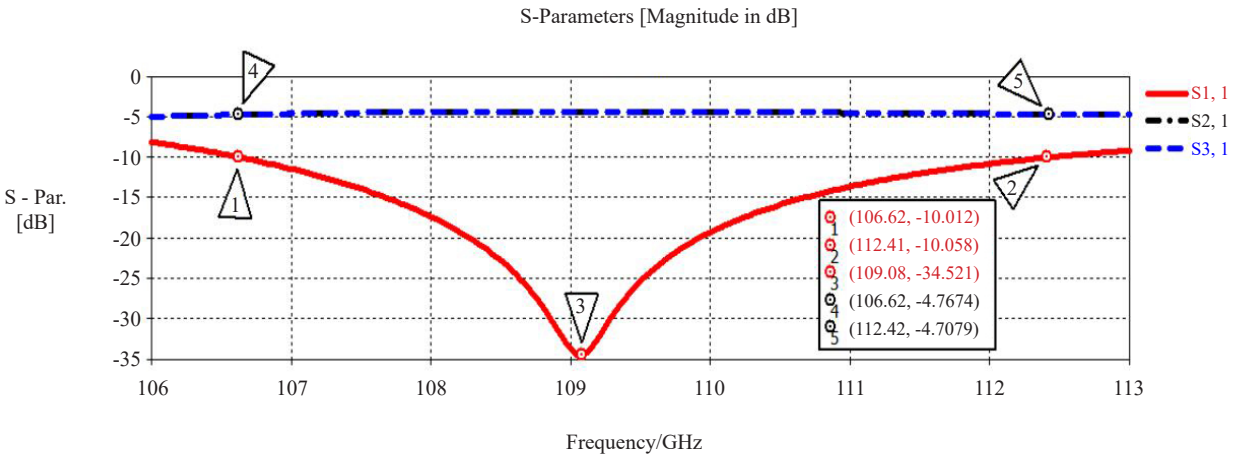

Figure 6. Simulation result of the S_{11} and the $S_{21} = S_{31}$ for the modeled SIW

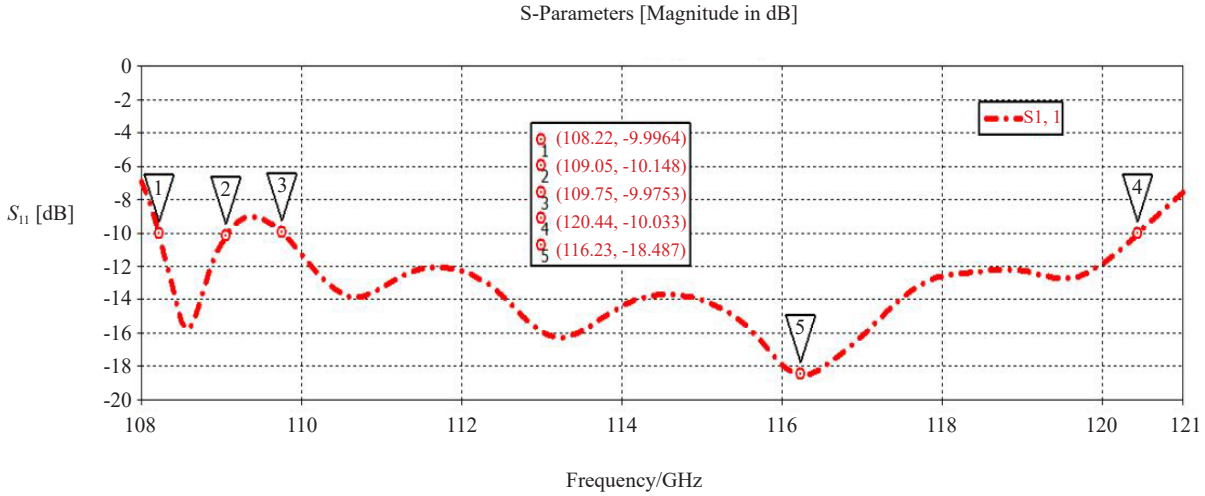

Figure 7. Simulation result of the S_{11} for the first offered 6G antenna

3.3 *Simulation results of the designed bandstop unit-cell FSS*

Figure 10 displays the simulation results of the S_{11} and S_{21} of the unit-cell stopband FSS. From this figure, it has been displayed that $S_{11} \leq$ -10 dB at 106.25-119.08 GHz, while $S_{21} <$ -0.52 dB at 106.45-119.29 GHz.

3.4 *Simulation results of the second offered 6G antenna*

Figure 11 displays the simulation result of the S_{11} of the second offered 6G antenna. From this figure, it has been displayed that the BW($S_{11} \leq$ -10 dB) = 11.86 GHz (10.38%), while the resonance frequency is 108.74 GHz.

Figures 12(a)-(c) display the simulation result of the 2D gain, 3D gain, and 3D directivity of the secondoffered 6G antenna. From Figure 12(a), it has been displayed that the gain was 14-25.53 dB at 105-121 GHz. From Figure 12(b), it has been displayed that the gain is equal to 25.53 dB @ 109 GHz. Lastly, from Figure 12(c), it has been displayed that directivity is equal to 26.9 dBi @ 109 GHz.

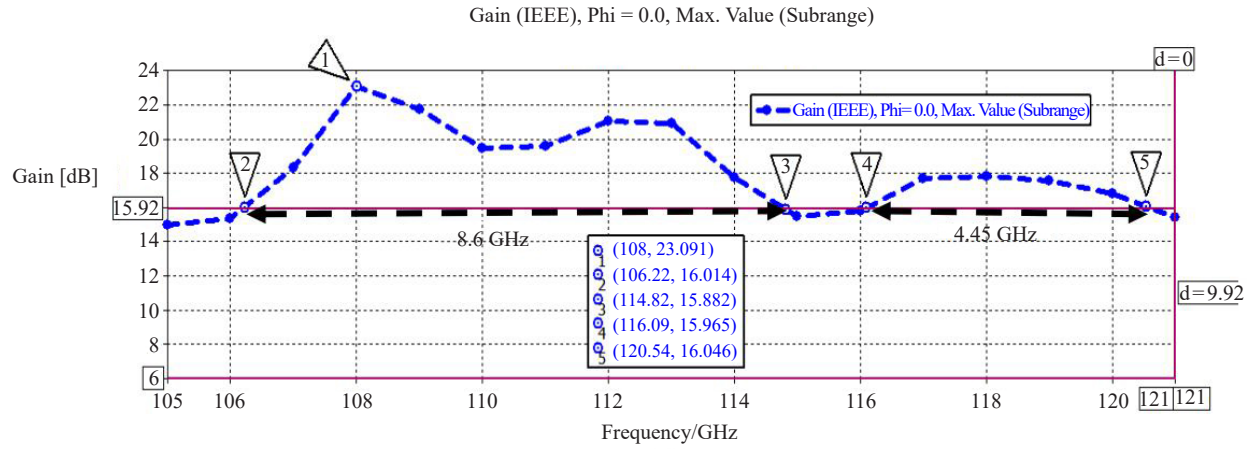

(a)

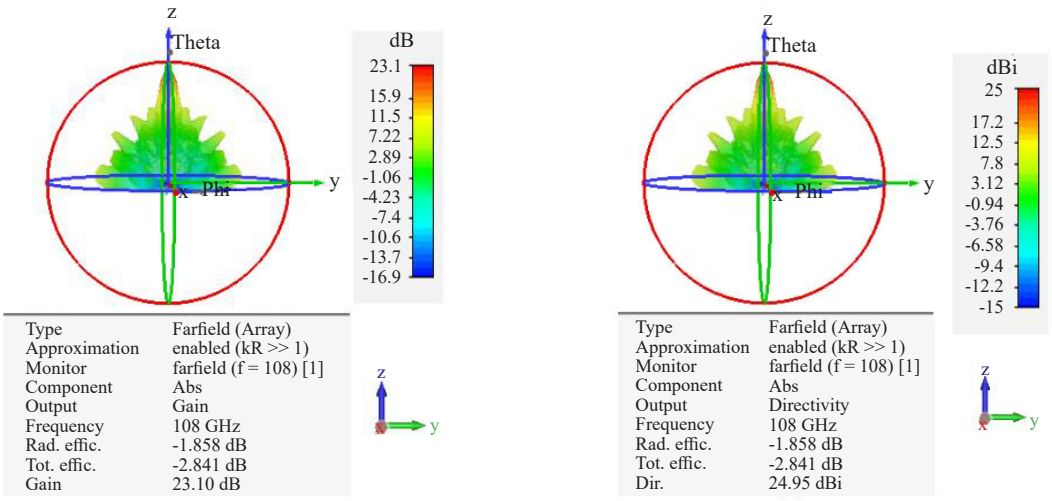

(b) (c)

Figure 8. Simulation results of the gain and the directivity for the first offered 6G antenna, (a) 2D gain, (b) 3D gain, (c) 3D directivity

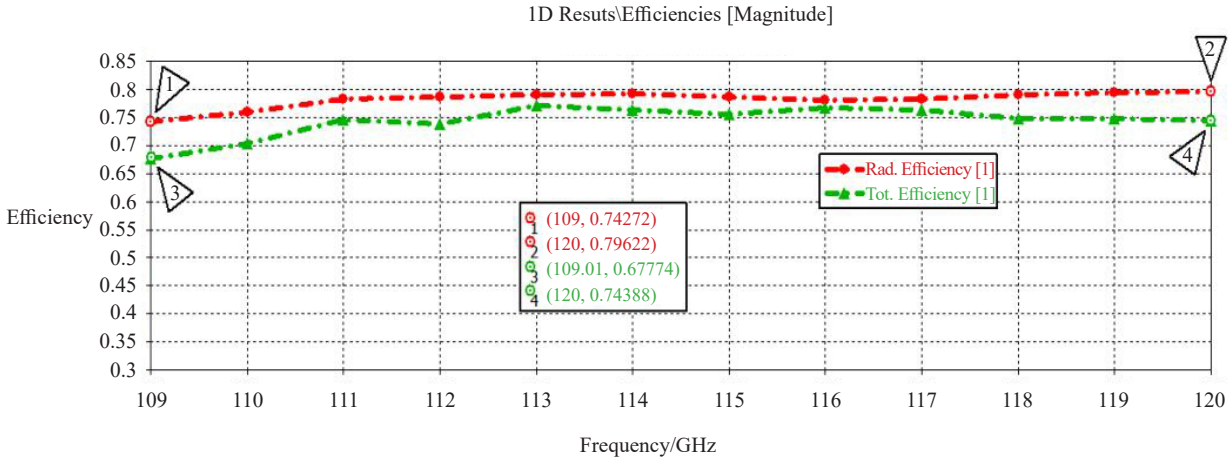

Figure 9. Simulation results of the total efficiency and radiation efficiency of the first offered 6G antenna

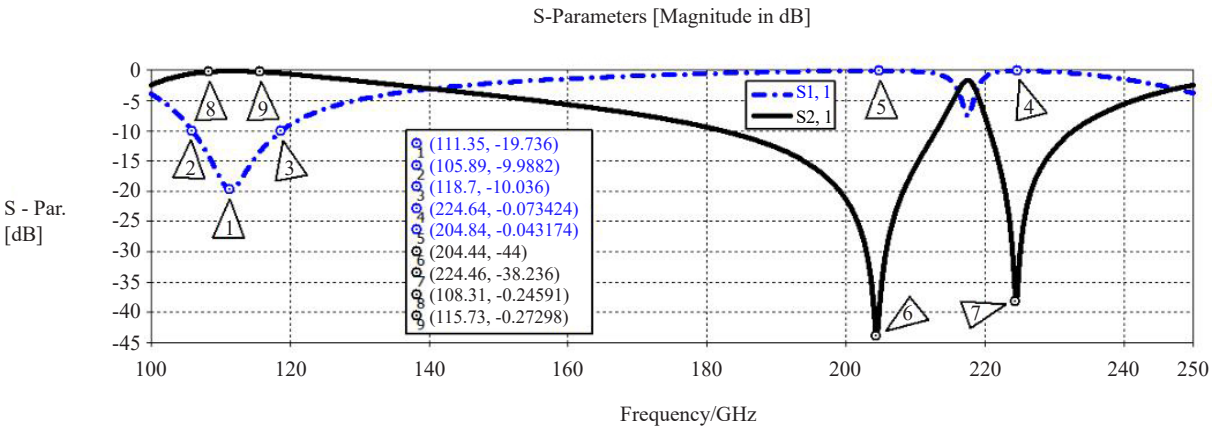

Figure 10. Simulation result of S_{11} and the S_{21} for the bandstop unit-cell FSS

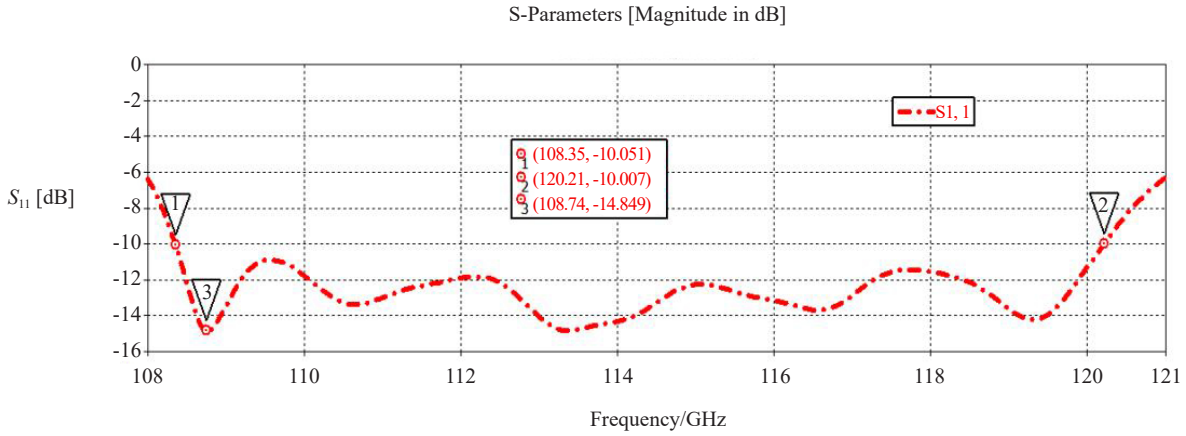

Figure 11. Simulation result of the S_{11} for the second offered 6G antenna

Figure 13 displays the simulation results of the radiation efficiency and total efficiency of the second offered 6G antenna. This figure displays that the radiation efficiency was 72.9-77.85 % at 109-120 GHz, while the total efficiency was 69.6-73.86% at 109-120 GHz.

Figures 14(a)-(b) display the comparison of gain and S_{11} between the first and the second offered 6G antennas. From Figure 14(a), it has been displayed that the gain within unit-cell stopband FSSs was more considerable by more than 3 dB at 108-110 GHz vs. without unit-cell stopband FSSs, and the peak change was 3.73 dB (at 109 GHz). Moreover, it has been displayed that inserting the unit-cell stopband FSSs into the antenna enhances the antenna's gain, almost at all frequency ranges 105-121 GHz. From Figure 14(b), it has been displayed that the BW increases by 0.34 GHz by embedding the modeled FSSs in the antenna.

3.5 *Correlation of the simulation results of the first offered 6G antenna with a couple of simulators*

An effective way to verify the results of antenna simulations is by validating and measuring with a manufactured prototype antenna. However, it is possible to do a simulation with two simulation software that works with different techniques, as is done in the articles [41]-[43], to get an approximate and cheaper estimate of the accuracy of the simulation results. We chose software validation/comparison in this paper as described above. Figure 15 displays the

correlation between the gain and S_{11} of the first offered 6G antenna attained from the Finite Integration Technique (FIT) solver within CST MWS and the Finite Element Method (FEM) solver within Ansys HFSS simulators. This figure displays that the peak gain and BW from the Ansys HFSS was about 25.3 dB, 12.5 GHz, while the peak gain and BW from the CST MWS was 23.1 dB, 11.5 GHz. So it has been displayed that a fair compromise betwixt the simulation results is attained concerning the first offered 6G antenna.

3.6 *Discussion*

This paper aimed to design a microstrip array antenna with SIW with dual outputs and WR-08 waveguide with or without FSSs. With more than 22 dBi directivity that can be used for 6G wireless communication networks at resonance frequencies above 107 GHz and software comparison with the Ansys HFSS software. In addition, in this research, we designed two 2 × 28 × 16 rectangular microstrip patch radiators in corporate-series fed microstrip antenna arrays, the first without FSSs and the second with FSSs, to further boost the antenna gain.

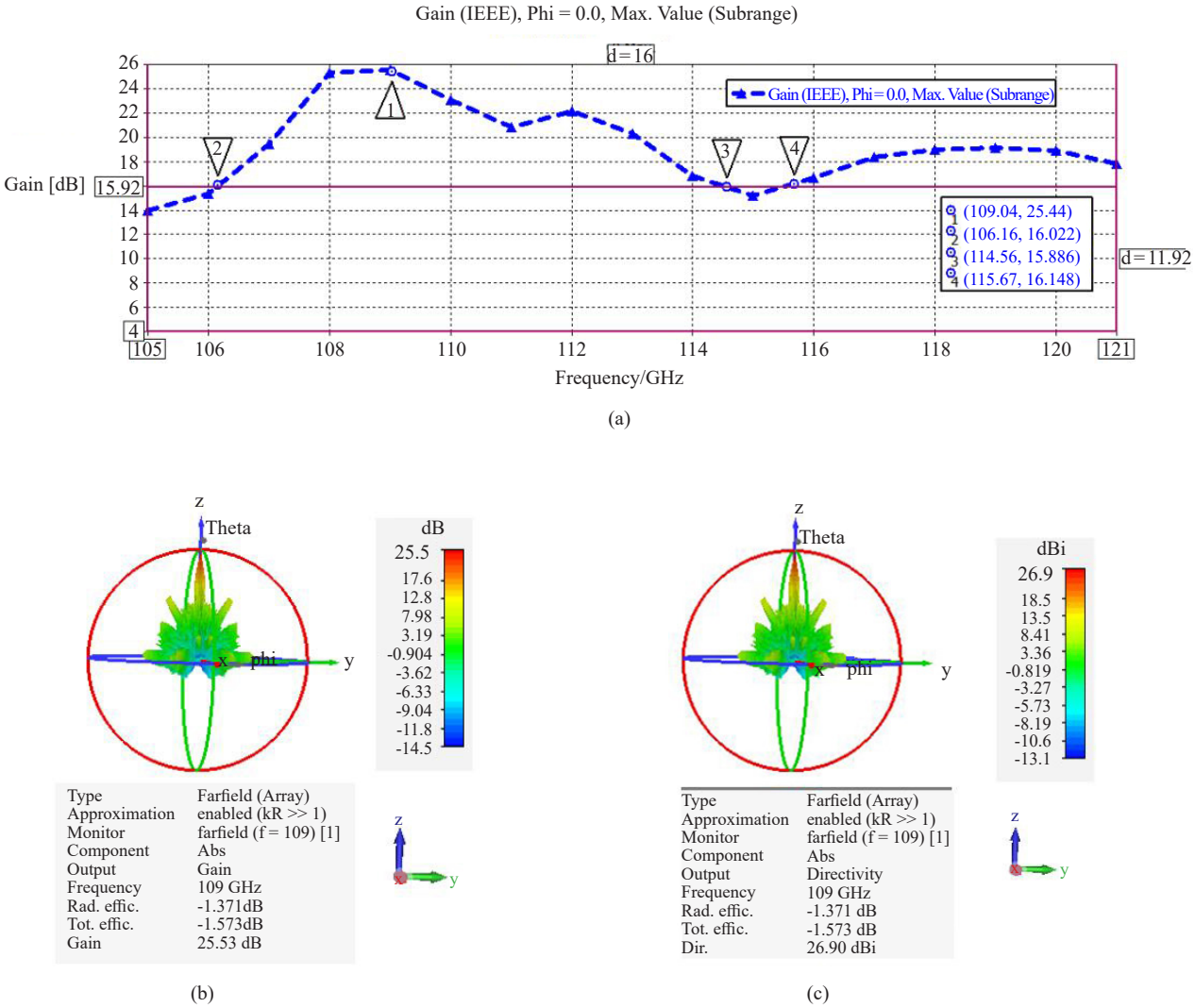

Figure 12. Simulation results of the gain and the directivity for the second offered 6G antenna, (a) 2D gain, (b) 3D gain, (c) 3D directivity

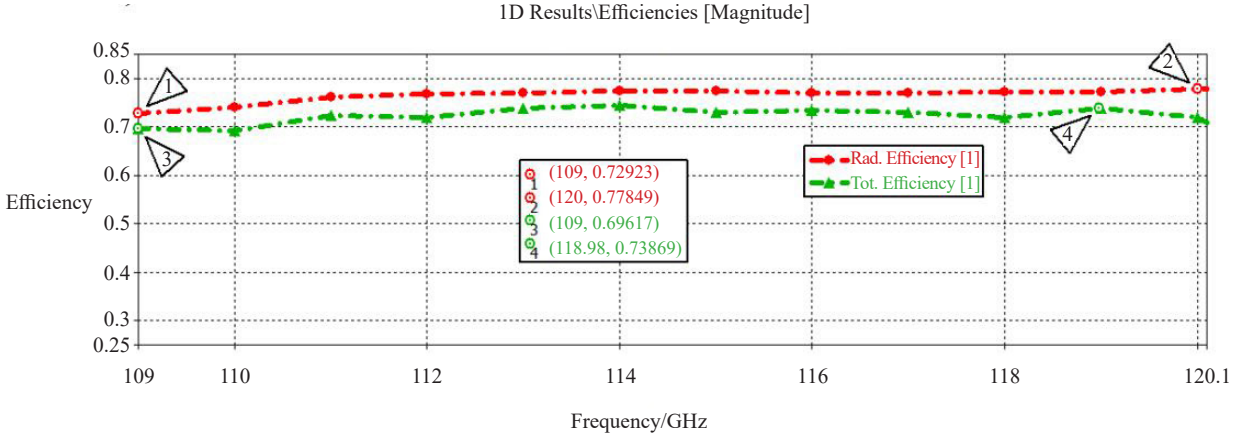

Figure 13. Simulation results for radiation and total efficiency of the second 6G offered antenna

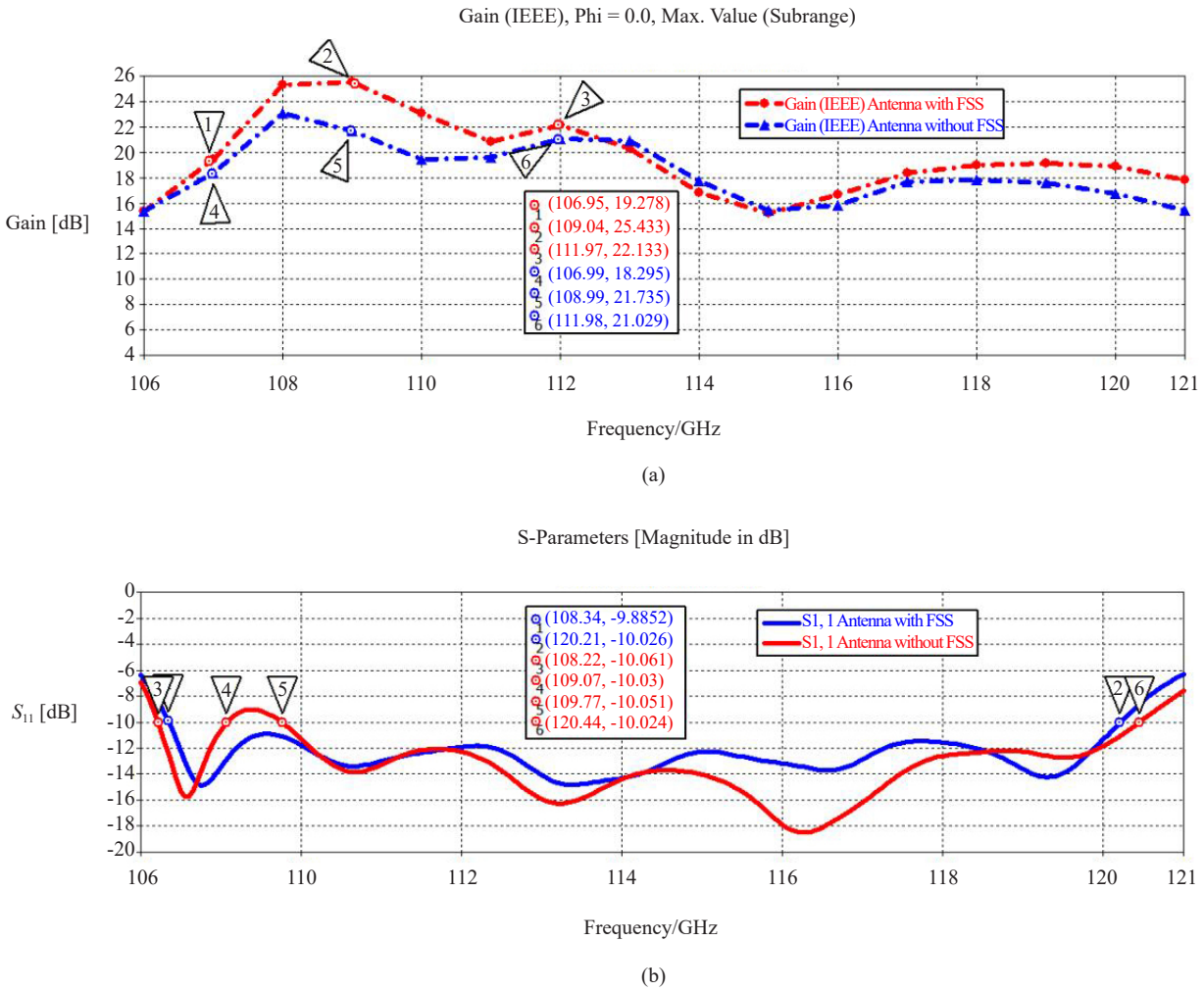

Figure 14. Comparison of simulation results between the first and the second offered 6G antennas, (a) Gain, (b) S_{11}

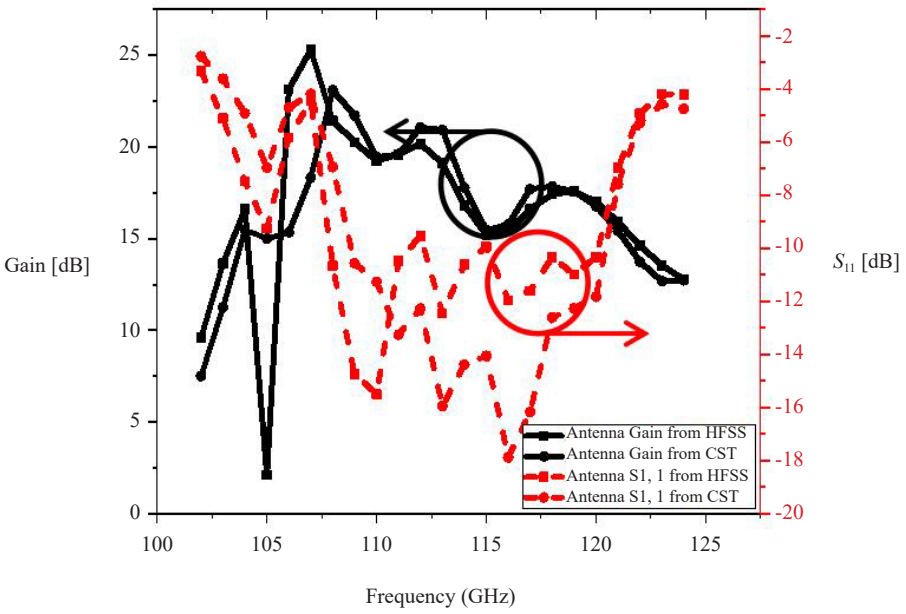

Figure 15. Simulation results from comparisons of the gain and the S_{11} of the first offered 6G antenna with the CST MWS and Ansys HFSS simulators

Following the simulation with CST MWS software, the peak directivity, gain, BW, peak radiation, and total peak efficiency attained for the microstrip array antennas without FSSs and with FSSs were 24.95 dBi, 23.1 dB, 11.52 GHz (10%), 79.6%, 74.4%, 26.9 dBi, 25.53 dB, 11.86 GHz (10.38%), 77.85%, and 73.86%, respectively. In order to diminish the surface waves, radiations, and conduction losses [35]-[37], the Rogers RO3003 has been used at the offered antennas with suitable laminate parameters [35]-[37].

The first design was simulated with the Ansys HFSS to compare the simulation results of this designed antenna simulated within the CST MWS, and the simulation results attained from the couple simulators were in fair compromise. It may have been displayed that these paperwork simulation results were validated within simulator validation and similar to that in [24], [41]-[43]. The simulation was done with the CST MWS, and validation was done with the Ansys HFSS, like work [24]. Unlike works [21]-[23], [25]-[27], the validation was done by the fabrication and measurement of the prototype original THz antenna, and in this work, the validation was by simulator comparison with the Ansys HFSS. The design and simulation in this work were done with the CST MWS. Unlike works [21]-[22], [25], [27]. While design and simulation in work [22] were done within the FEKO simulator and the designs in paperwork [21], [25], [27] were done within the Ansys HFSS. Unlike works [21]-[27], where one antenna was designed, while at this paperwork, dual antennas were designed, and the second antenna had larger BW and directivity. Unlike the paperwork [21]-[25], the unit-cell bandstop FSSs enhance the antenna gain in this paperwork. This paperwork attained the highest and steady total radiation efficiency for the microstrip laminated found antenna equal to the different paperwork [21]-[22]. Similar to what was done in works [2]-[5] that relate to 5G cellular communication in the sub-6GHz frequencies range to improve the performance of the 5G cellular communication system in terms of capacity and data rate by using MtM and CRLH technique, this work an array FSSs technique, which is similar to the MtM and CRLH techniques is used to increase the BW and the gain of our proposed antenna for 6G cellular communication to improve the performance of the future communication system, on the other hand in works [2]-[3], [6]-[7] MIMO, beam steering and reconfigurable are used, respectively, to improve the performance of the 5G communication system when such use can be made in future works for 6G cellular systems. Table 1 compares different papers with this paper.

Table 1. Comparison with different papers

Paper	Techno.	Reson. Freq. (GHz)	BW (GHz/%)	Peak Direc./gain (dBi/dB)	Peak Rad./Total Effici. (%)	Validation
[21]	On-chip SIW antenna	550	20 GHz/3.63%	9.4 dBi/2.8 dB	22	Experimental
[22]	400-GHz FRA antenna	400	64 GHz/16%	33.66 dBi	Aperture effici. = 33.65	Experimental
[23]	Elliptical lens fed by LWA	180	80 GHz/40%	35.8 dBi	Aperture effici. = > 80	Experimental
[24]	Dipole antenna with three directors on BCB and InP substrates	300	116 GHz/38.6%	8.44 dBi/8.01 dB	n/a	Ansys HFSS
[25]	V-shaped on-chip microstrip antenna	280	80 GHz/28.7%	11 dBi/5.48 dB	28	Experimental
[26]	Metallic lens antenna	415	90 GHz/21.68%	29.1 dBi	n/a	Experimental
[27]	Quasi-planar reflector antenna	412.5	175 GHz/42%	32 dB	64.9	Experimental
This work	2 × 20 × 16 microstrip array antenna with SIW	116.25	11.52 GHz/10%	24.95 dBi/23.1 dB	79.6/74.4	Ansys HFSS
	2 × 20 × 16 microstrip array antenna with SIW and FSSs	108.95	11.86 GHz/10.38%	26.9 dBi/25.53 dB	77.85/73.86	

4.Conclusions

The microstrip array 6G antennas designed by CST MWS software included SIW with dual outputs and WR-08 waveguide at a nominal frequency of beyond 107 GHz and compared the simulation results by Ansys HFSS software. The first antenna was without FSSs, while the second antenna was with the FSSs. As a result, this comparison's peak gain and BW for the first antenna were 25.3 dB, 12.5 GHz, 23.1 dB, and 11 GHz within Ansys HFSS and the CST MWS, correspondingly. The investigated results reveal that the proposed antennas may be employed as a 6G wireless communication network base. First, however, experimental verification with the manufacture of an archetype 6G antenna and measurement must be accomplished to achieve more accurate and precise verification. As future work, this work can include the MIMO or beam steering or the reconfigurable capabilities for developing smart planar microstrip antennas for 6G wireless communication networks.

Conflict of interest

The authors declare no competing financial interest.

References

[1] D. Milovanovic and Z. Bojkovic, "5G mobile networks: what is next?" *International Journal of Communications*, vol. 4, pp. 1-5, 2019.

[2] S. H. Ghadeer, S. K. A. Rahim, M. Alibakhshikenari, B. S. Virdee, T. A. Elwi, A. Iqbal, and M. AlHasan, "An innovative fractal monopole MIMO antenna for modern 5G applications," *AEU-International Journal of Electronics and Communications*, vol. 159, no. 154480, pp. 1-16, 2023.

[3] H. H. Al-Khaylani, T. A. Elwi, and A. A. Ibrahim, "Optically remote-controlled miniaturized 3D reconfigurable CRLH-printed MIMO antenna array for 5G applications," *Microwave Optical Technology Letters*, vol. 65, no. 2,

pp. 603-610, 2022.
[4] M. Haleem and T. A. Elwi, "Circularly polarized metamaterial patch antenna circuitry for modern applications," *International Journal of Emerging Technology and Advanced Engineering*, vol. 12, no. 12, pp. 44-50, 2022.
[5] M. M. Ismail, T. A. Elwi, and A. J. Salim, "A miniaturized printed circuit CRLH antenna-based Hilbert metamaterial array," *Journal of Communication Software and Systems*, vol. 18, no. 3, pp. 236-243, 2022.
[6] Z. S. Muqdad, M. Alibakhshikenari, T. A. Elwi, Z. A. A. Hassain, B. S. Virdee, R. Sharma, S. Khan, N. T. Tokan, P. Livreri, F. Falcone, and E. Limiti, "Photonic-controlled metasurface for intelligent antenna beam steering applications including 6G mobile communication systems," *AEU-International Journal of Electronics and Communications*, vol. 166, no. 154652, pp. 1-18, 2023.
[7] S. T. Al-Hadeethi, T. A. Elwi, and A. A. Ibrahim, "A printed reconfigurable monopole antenna based on novel metamaterial structures for 5G applications," *Micromachines*, vol. 14, no. 131, pp. 1-14, 2023.
[8] S. Elmeadawy and R. M. Shubair, "6G wireless communications: future technologies and research challenges," In IEEE International Conference on Electrical and Computing Technologies and Applications (ICECTA), Ras Al Khaimah, United Arab Emirates, 19-21 Nov. 2019, pp. 1-5.
[9] M. Z. Chowdhury, M. Shahjalal, S. Ahmed, and Y. M. Jang, "6G wireless communication systems: applications, requirements, technologies, challenges, and research directions," *IEEE Open Journal of the Communications Society*, vol. 1, pp. 957-975, 2020.
[10] W. Saad, M. Bennis, and M. Chen, "A vision of 6G wireless systems: applications, trends, technologies, and open research problems," *IEEE Network*, vol. 34, no. 3, pp. 134-142. 2019.
[11] C. Han, Y. Wu, Z. Chen, and X. Wang, "Terahertz communications (TeraCom): challenges and impact on 6G wireless systems," *arXiv*, pp. 1-8, 2019. Available: https://doi.org/10.48550/arXiv.1912.06040 [Accessed May 5, 2019].
[12] E. C. Strinati, S. Barbarossa, J. L. Gonzalez-Jimenez, D. Kténas, N. Cassiau, and C. Dehos, "6G: the next frontier," *arXiv* [E-prints], pp. 1-16, 2019. Available: https://doi.org/10.48550/arXiv.1901.03239 [Accessed May 10, 2019].
[13] T. S. Rapport, Y. Xing, O. Kanhere, S. Ju, A. Madanayake, S. Mandal, A. Alkhateeb, and G. C. Trichopoulos, "Wireless communications and applications above 100 GHz: opportunities and challenges for 6G and beyond," *IEEE Access*, vol. 7, pp. 78729-78757, 2019.
[14] W. Aman, M. M. U. Rahman, H. T. Abbas, M. A. Khalid, M. A. Imran, A. Alomainy, and Q. H. Abbasi, "Securing the insecure: a first-line-of-defense for nanoscale communication systems operating in THz band," *arXiv* [Preprint], pp. 1-7, 2020. Available: https://doi.org/10.48550/arXiv.2007.06818 [Accessed Mar. 3, 2020].
[15] K. R. Jha and G. Singh, *Terahertz Planar Antennas for Next-Generation Communication*. Cham, Switzerland: Springer International Publishing, 2014.
[16] K. Tekbiyik, A. R. Ekti, G. K. Kurt and A. Gorcin, "Terahertz band communication systems: challenges, novelties, and standardization efforts," *Physical Communication*, vol. 35, no. 100700, pp. 1-28, 2019.
[17] I. F. Akyildiz, C. Han, and S. Nie, "Combating the distance problem in the millimeter-wave and terahertz frequency bands," *IEEE Communications Magazine*, vol. 56, no. 6, pp. 102-108, 2018.
[18] C. Han and Y. Chen, "Propagation modeling for wireless communications in the terahertz band," *IEEE Communications Magazine*, vol. 56, no. 6, pp. 96-101, 2018.
[19] M. Fujishima, "Key technologies for THz wireless link by silicon CMOS integrated circuits," *Photonics*, vol. 5, no. 4, pp. 50, 2018.
[20] H. Sarieddeen, M. S. Alouini, and T. Y. Al-Naffouri, "Terahertz-band ultra-massive spatial modulation MIMO," *IEEE Journal on Areas in Communication*, vol. 37, no. 9, pp. 2040-2052, 2019.
[21] K. Dhwaj, Y. Zhao, R. A. Hadi, X. Li, F. M. C. Chang, and T. Itoh, "A 0.55 THz on-chip substrate integrated waveguide antenna," In 2018 43rd International Conference on Infrared, Millimeter, and Terahertz Waves (IRMMW-THz), Nagoya, Japan, 2018, pp. 1-2.
[22] Z. W. Miao, Z. C. Hao, Y. Wang, B. B. Jin, J. B. Wu, and W. Hong, "A 400-GHz high-gain quartz-based single-layered folded reflectarray antenna for terahertz applications," *IEEE Transaction on Terahertz Science and Technology*, vol. 9, no. 1, pp. 78-88, 2019.
[23] D. B. Montero, M. A. Campo, and N. Llombart, "Broadband low-permittivity elliptical lens fed by a leaky-wave antenna for communications applications," In 2018 43rd International Conference on Infrared, Millimeter, and Terahertz Waves (IRMMW-THz), Nagoya, Japan, 2018, pp. 1-2.
[24] H. Vettikalladi, W. T. Sethi, M. A. Alkanha, and M. Himdi, "Sub-THz dipole antenna for future 5G wireless communication," In 2019 2nd International Conference on Computer Applications & Information Security (ICCAIS), Riyadh, Saudi Arabia, 2019, pp. 1-4.

[25] H. Kim, W. Choe, and J. Jeong, "A terahertz CMOS V-shaped patch antenna with defected ground structure," *Sensors*, vol. 18, no. 8, pp. 2432, 2018.
[26] Z. C. Hao, J. Wang, Q. Yuan, and W. Hong, "Development of a low-cost THz metallic lens antenna," *IEEE Antennas and Wireless Propagation Letters*, vol. 16, pp. 1751-1754, 2017.
[27] K. Fan, Z. C. Hao, Q. Yuan, and W. Hong, "Development of a high gain 325-500 GHz antenna using quasi-planar reflectors," *IEEE Transaction on Antennas and Propagation*, vol. 65, no. 7, pp. 3384-3391, 2017.
[28] K. Wu and Y. Cassivi, "The substrate integrated circuits- a new concept for high-frequency electronics and optoelectronics," In 6th International Conference on Telecommunications in Modern Satellite, Cable and Broadcasting Service, TELSIKS 2003, Nis, Yugoslavia, 2003, pp. P-III.
[29] G. Q. Luo, T. Y. Wang, and X. H. Zhang, "Review of low-profile substrate integrated waveguide cavity-backed antennas," *International Journal of Antennas and Propagation*, vol. 2013, no. 746920, 2013.
[30] Y. Arfat, S. P. Singh, S. Khan, and S. Arya, "Modelling and design of substrate integrated waveguide using two parallel rows of rectangular conducting slots," *International Journal of Current Engineering and Technology*, vol. 3, no. 5, pp. 2101-2103, 2013.
[31] V. Zhurbenko, *Passive Microwave Components, and Antennas*. Vukovar, Croatia: InTech, 2010, pp. 226-246.
[32] T. Djerafi, A. Doghri, and K. Wu, *Handbook of Antenna Technologies: Substrate Integrated Waveguide Antennas*. Singapore: Springer, 2015.
[33] A. Kishk, *Advancement in Microstrip Antennas with Recent Applications*. Vukovar, Croatia: In-Tech, 2013.
[34] U. Nissanov, G. Singh, and N. Kumar, "High gain microstrip array antenna with SIW and FSS for beyond 5G at THz band," *Optik*, vol. 236, pp. 166568, 2021.
[35] J. D. Preez and S. Sinha, *Millimeter-Wave Antennas: Configurations and Applications*. Switzerland: Springer, 2016.
[36] G. Kouemou, *Radar Technology*. Vukovar, Croatia: InTech, 2009.
[37] L. K. S. Granados, "Antennas for millimeter-wave applications," Ph. D. Thesis, Instituto Nacional de Astrofísica, Ópticay Electrónica (INAOE), Mexico, 2016.
[38] G. F. Hamberger, U. Siart, and T. F. Eibert, "A broadband low-loss WR10 waveguide to microstrip line transition with T-shaped probe," *Progress in Electromagnetics Research Letters*, vol. 73, pp. 17-22, 2018.
[39] O. Khan, J. Pontes, X. Li., and C. Waldschmidt, "A wideband variable-width microstrip grid array antenna," In 2014 44th European Microwave Conference, Rome, Italy, 2014, pp. 1644-1647.
[40] M. S. Esfahlan and I. Tekin, "77 GHz PCB patch antenna," In URSI-TURKİYE, Ankara, Turkey, 2016, pp. 1-3.
[41] U. Nissanov and G. Singh, "High directivity microstrip antenna with stopband and passband FSSs for 6G at low-THz," *International Journal of Electrical and Computer Engineering*, vol. 12, no. 6, pp. 6272-6283, 2022.
[42] U. Nissanov, "6G Rotman lens D-band beam-steering microstrip antenna," *Journal of Computational Electronics*, vol. 21, no. 2, pp. 431-444, 2022.
[43] U. Nissanov, G. Singh, and A. Akinola, "Sixth-generation (6G) microstrip antenna with high-gain," *International Journal on Communications Antenna and Propagation (IRECAP)*, vol. 11, no. 4, pp. 279-287, 2021.